

Element Synthesis in Stars

F.-K. Thielemann, F. Brachwitz, C. Freiburghaus, E. Kolbe,
G. Martinez-Pinedo, T. Rauscher, F. Rembgas
Department of Physics & Astronomy, Univ. of Basel,
Klingelbergstrasse 82, CH-4056 Basel, Switzerland

W.R. Hix, M. Liebendörfer, A. Mezzacappa
Physics Division, Oak Ridge National Laboratory,
Oak Ridge, TN 37831-6371, USA

K.-L. Kratz, B. Pfeiffer
Institut für Kernchemie, Univ. Mainz, Fritz-Strassmann-Weg 2,
D-55099 Mainz, Germany

K. Langanke
Institute of Physics and Astronomy, University of Aarhus,
DK-8000 Aarhus C, Denmark

K. Nomoto
Department of Astronomy, University of Tokyo,
Tokyo 113-0033, Japan

S. Rosswog
Department of Physics and Astronomy, University of Leicester,
University Road, LE1 7RH, Leicester, UK

H. Schatz
National Superconducting Cyclotron Laboratory & Department of Physics
and Astronomy, Michigan State University, East Lansing, MI 48824

M. Wiescher
Department of Physics, University of Notre Dame,
Notre Dame, IN 46556, USA

Abstract

Except for ^1H , ^2H , ^3He , ^4He , and ^7Li , originating from the Big Bang, all heavier elements are made in stellar evolution and stellar explosions. Nuclear physics, and in many cases nuclear structure far from stability, enters in a crucial way. Therefore, we examine in this review the role of nuclear physics in astrophysics in general and in particular how it affects stellar events and the resulting nucleosynthesis. Stellar modeling addresses four major aspects: 1. energy generation and nucleosynthesis, 2. energy transport via conduction, radiation or possibly convection, 3. hydrodynamics/hydrostatics, and finally 4. thermodynamic properties of the matter involved. Nuclear Physics enters via nuclear reaction cross sections and nuclear structure (affecting the composition changes and nuclear energy generation), neutrino-nucleon and neutrino-nucleus cross sections (affecting neutrino opacities and transport), and e.g. the equation of state at and beyond nuclear densities which creates a relation between the nuclear many body problem and hydrodynamic response like pressure and entropy. In the following we review these four topics by highlighting the role and impact of nuclear physics in each of these aspects of stellar modeling. The main emphasis is put on the connection to element synthesis.

1 Introduction

The most dominant influence of nuclear physics on element synthesis is given by nuclear reactions occurring in a stellar environment. Different stellar environments also require different kinds of nuclear physics knowledge. In stellar evolution all types of fusion reactions transform hydrogen to iron-group nuclei via hydrogen, helium, carbon, neon, oxygen and silicon burning, releasing eventually 8.7 MeV of binding energy per nucleon. The composition changes in stellar evolution, occurring on timescales of millions to billions of years rather than timescales of the strong interaction are dominated by reactions which can barely proceed for the temperatures involved. The latter correspond to typical bombarding energies below the Coulomb barrier. The study of such reactions needs high intensity, (very) low energy beams and either passive or active shielding [37, 3]. For more details and updates see the contribution by C.Rofls [89].

Reactions occurring in explosive environments experience higher temperatures and thus higher bombarding energies and larger cross sections. The fact that shorter explosive timescales permit reactions for unstable nuclei before their decay makes it necessary to investigate also cross sections with unstable nuclei. For experimental methods and reviews see e.g. Refs. [37, 2]. Theoretical predictions involving nuclei at excitations with a sufficiently high density of states, i.e. permitting the application of the statistical model, are reviewed in [78, 79], with a special attention of including isospin mixing, level densities and alpha potentials. The state of the art in weak interaction predictions, especially for electron capture on nuclei and the application of the shell model for large model spaces is discussed in [46]. Many explosive environments with fuels of $N \approx Z$ produce also unstable nuclei close to stability. However, explosive environments with a large surplus of hydrogen (protons) permit proton captures up to the proton dripline. This gives rise to the so-called rp-process (rapid proton capture). Early ignition stages lead to break-out reactions from reaction cycles similar to the hot CNO [85], so-called two-proton capture reactions via an intermediate proton-unstable nucleus can play an essential role [93]. Very neutron-rich environments permit neutron-captures up to the neutron dripline and are the sites of the r-process (rapid neutron capture). Nuclear structure far from stability enters directly [42], but also features like pygmy resonances in the E1-strength at low energies (due to extended neutron skins) can have a decisive influence on the size of neutron capture cross sections [22].

Composition changes in astrophysical environments at low and intermediate temperatures are described by individual cross sections to follow the reaction flows. High temperatures lead to chemical equilibria. In the case of the rp- and r-process this causes abundance distributions on isotonic or isotopic lines which show maxima at specific proton or neutron separation energies. Therefore, in such cases individual reactions might not be that important, but such equilibria depend on correct reaction Q-values or separation energies, i.e. the proper knowledge of nuclear masses far from stability. The behavior of shell effects and shell closures deserves special attention [42], see also the contribution by W. Nazarewicz [63]. The tendency in recent years is here to move from macroscopic-microscopic models like the droplet model to non-relativistic or relativistic mean field methods and even shell model calculations, if the model space permits this [60, 14, 44, 54]. Another aspect in the r-process is related to fission barriers and fission yields for nuclei far from stability [11, 52, 70].

While strong interaction timescales can support equilibria at high temperatures (and densities), weak interactions lead very seldom to chemical equilibria. Exceptions are early phases of the big bang and equilibrated (cooled) neutron stars. Thus, it is always necessary to follow each individual weak interaction, i.e. beta-decays, electron captures and neutrino-nucleus interactions. The present state of the art calculations for beta-decays are QRPA or shell model calculations [61, 54], electron capture calculations are now possible within the shell model up to the pf-shell, i.e. the important Fe-group nuclei [46]. The best calculations for neutrino-nucleus cross sections are available within the continuum RPA (CRPA) model [39, 27, 45, 40].

Most of the modes responsible for energy transport in stellar environments are not nuclear physics related: mixing/convection of matter with a given heat content or transport via radiation (photons). The first category involves all types of hydrodynamic instabilities from convection due to entropy inversion in regular stellar evolution [25] to Rayleigh-Taylor instabilities in dynamic events [64, 65] and rotationally induced meridional circulation [53]. Radiation transport is governed by photon scattering and reaction processes. Photon-ion interactions with bound-bound and bound-free transitions are covered in atomic physics and generally addressed as opacities. In a similar way photon-electron interactions enter [88]. Nuclear physics is addressed when "radiation" transport proceeds by the way of neutrinos in hot neutron star environments, be it in stellar collapse in supernovae or events which involve hot neutron stars collapsing to black holes (either in massive stars or in neutron star mergers) [58]. Here the cross sections of neutrino-nucleus, neutrino-nucleon, neutrino-nuclear matter and neutrino-electron/positron collisions are relevant and the quest is to perform precise calculations [6, 7, 73, 116].

Hydrodynamics is an essential feature in any stellar modeling, be it in 1D (mostly spherically symmetric) [59] or 2D and 3D [35, 64, 65], multigrid or adaptive grid methods [15], making use of implicit vs. explicit numerical methods [29], or employing general relativity rather than Newtonian hydrodynamics [49, 50]. For these issues, however, there exists no direct relation to nuclear physics properties, unless one considers how timescales of nuclear energy release can enter hydrodynamic modeling. Nevertheless, hydrodynamics provides the environment conditions which determine nuclear reactions, composition changes and thus also energy generation.

Convection and radiation transport are both closely linked to the numerical treatment of hydrodynamics. How are convective flows modeled in 1D

vs. multi-D hydro? Which methods are employed to perform radiation transport, independent on the micro-physics related cross sections involved? Two of the schemes employed in neutrino transport are flux-limited diffusion or more recently full transport via solving the Boltzmann transport equation [57, 58].

Thermodynamics is an aspect also coupled strongly to hydrodynamics, as the pressure due to the equation of state enters directly into the formation of shock waves, the entropy enters into the formation of hydrodynamical instabilities and convection. In the outer zones of a star, especially the atmosphere, the EOS is mainly given by atomic physics via the mixture of a partially ionized ion, electron, and photon gas [12]. In deeper layers ions are fully ionized and the thermalized Fermi gases (e.g. electron/positron), Bose gases of massless particles (i.e. Planck distributions of photons) and Boltzmann distributions of nuclei are needed. Here nuclear physics enters only indirectly by possibly governing the reactions which provide the composition of nuclei and the total amount of electrons available, the latter being dependent on electron captures and weak interactions in general.

A more direct involvement of nuclear physics is given for the EOS at and beyond nuclear densities ρ_0 [74, 47, 94]. Important features are the different stages of dissolving nuclei into a nucleon soup (involving a number of topologies) and the creation of new particles at supranuclear densities. When do hyperons occur (sigmas, lambdas at $2 \times \rho_0$?), do we have a formation of kaon or pion condensates, at what density does the quark-hadron phase transition occur ($4-5 \times \rho_0$?) [108]?

After this short general introduction and overview, we want to discuss a number of specific astrophysical applications to show how the different nuclear aspects affect the synthesis of elements in the modeling of stellar events. In particular we address stellar evolution, type II and type Ia supernovae (SNe II and SNe Ia), novae and X-ray bursts (the sites of explosive H-burning and the rp-process), and the features and possible sites of the r-process.

2 Stellar Evolution

2.1 The Role of Individual Reactions

H-burning converts ${}^1\text{H}$ into ${}^4\text{He}$ via pp-chains or the CNO-cycles. The simplest PPI chain is initiated by ${}^1\text{H}(p, e^+\nu){}^2\text{H}(p, \gamma){}^3\text{He}$ and completed by ${}^3\text{He}({}^3\text{He}, 2p){}^4\text{He}$. The dominant CNO-I cycle chain ${}^{12}\text{C}(p, \gamma){}^{13}\text{N}(e^+\nu){}^{13}\text{C}(p, \gamma){}^{14}\text{N}(p, \gamma){}^{15}\text{O}(e^+\nu){}^{15}\text{N}(p, \alpha){}^{12}\text{C}$ is controlled by the slowest reaction ${}^{14}\text{N}(p, \gamma){}^{15}\text{O}$. Further burning stages are characterized by their major reactions, which are in He-burning ${}^4\text{He}(2\alpha, \gamma){}^{12}\text{C}$ (triple-alpha) and ${}^{12}\text{C}(\alpha, \gamma){}^{16}\text{O}$, in C-burning ${}^{12}\text{C}({}^{12}\text{C}, \alpha){}^{20}\text{Ne}$, and in O-burning ${}^{16}\text{O}({}^{16}\text{O}, \alpha){}^{28}\text{Si}$. The alternative to fusion reactions are photodisintegrations which start to play a role at sufficiently high temperatures when $30kT \approx Q$ (the Q-value or energy release of the inverse capture reaction). This ensures the existence of photons with energies $>Q$ in the Planck distribution and leads to Ne-Burning [${}^{20}\text{Ne}(\gamma, \alpha){}^{16}\text{O}$, ${}^{20}\text{Ne}(\alpha, \gamma){}^{24}\text{Mg}$] at $T > 1.5 \times 10^9\text{K}$ (preceding O-burning) due to a small Q-value of ≈ 4 MeV and Si-burning at temperatures in excess of $3 \times 10^9\text{K}$ (initiated like Ne-burning by photodisintegrations of ${}^{28}\text{Si}$). The latter ends in a chemical equilibrium with an abundance distribution around Fe (nuclear statistical equilibrium, NSE), as typical Q-values of 8–10 MeV permit photodisintegrations as well as the penetration of the corresponding Coulomb barriers at these temperatures. Stars with masses $M > 8M_\odot$ develop an onion-like composition structure, after passing through all hydrostatic burning stages, and produce a collapsing core at the end of their evolution, which proceeds to nuclear densities [66, 113, 8, 25, 106, 26]. Less massive stars experience core H- and He-burning and end as C/O white dwarfs after strong episodes of mass loss [23]. These do not exceed the Chandrasekhar mass, i.e. the maximum stellar mass stabilized against contraction due to the pressure of the degenerate electron gas.

The major uncertainties in all these hydrostatic burning stages are related to low energy fusion reactions, i.e. the cross sections at sub Coulomb barrier energies, where (until recently) a determination could be only obtained by extrapolation to low energies. The status of reactions has been discussed extensively [37, 1] and is presented in the most recent compilation [2]. The main breakthrough in recent years is due to the possibility of measuring cross sections at stellar thermal energies in underground laboratories (LUNA) [3, 89]. A number of uncertain reactions at low energies still wait to be explored with the aid of this new and promising method.

2.2 Weak Interactions and Electron Captures

The late phases of stellar evolution (O- and Si-burning) are less prone to cross section uncertainties from strong interactions due to the emergence of equilibria, as discussed above. However, the high densities result in partially or fully degenerate electrons with increasing Fermi energies [66]. When these supercede the Q-value thresholds of electron capture reactions, this allows for electron capture on an increasing number of initially Si-group and later Fe-group (pf-shell) nuclei. Because sd-shell reactions were well understood in the past [20], O-burning results are quite safe. The recent progress in pf-shell rates [46] led to drastic changes in the late phases of Si-burning [26], thus also setting new conditions for the subsequent Fe-core collapse after Si-burning, the size of the Fe-core and its electron fraction $Y_e = \langle Z/A \rangle$ [55].

3 Massive Stars and Type II Supernovae

3.1 The Explosion Mechanism

Electron captures on pf-shell nuclei (and later on free protons!) in the central Fe-core, resulting from preceding Si-burning, trigger a pressure decrease and the collapse of the Fe-core. The size of the homologously collapsing core (where infall velocities are proportional to the radius), which turns into nuclear matter during bounce [74], is dependent on the amount of prior electron captures on pf-shell nuclei [55, 26]. The total energy released, $2\text{--}3 \times 10^{53}$ erg, equals the gravitational binding energy of a neutron star and is thus dependent on the nuclear equation of state (EOS) [74] which determines the central density. Fig. 1 shows a sequence of density profiles during collapse, bounce, and shortly thereafter [59, 49], performed with the Lattimer & Swesty EOS [47].

Because neutrinos are the particles with the longest mean free path, they are able to carry away that energy in the most rapid fashion as seen for SN1987A in the Kamiokande, IMB and Baksan experiments. The apparently most promising mechanism for supernova explosions is based on neutrino heating beyond the hot proto-neutron star via the dominant processes $\nu_e + n \rightarrow p + e^-$ and $\bar{\nu}_e + p \rightarrow n + e^+$ with a (hopefully) about 1% efficiency in energy deposition [35, 58]. The neutrino heating efficiency depends on the neutrino luminosity, which in turn is affected by neutrino opacities [6, 7, 73], where also inelastic neutrino scattering on nuclei [39, 45] contributes. The

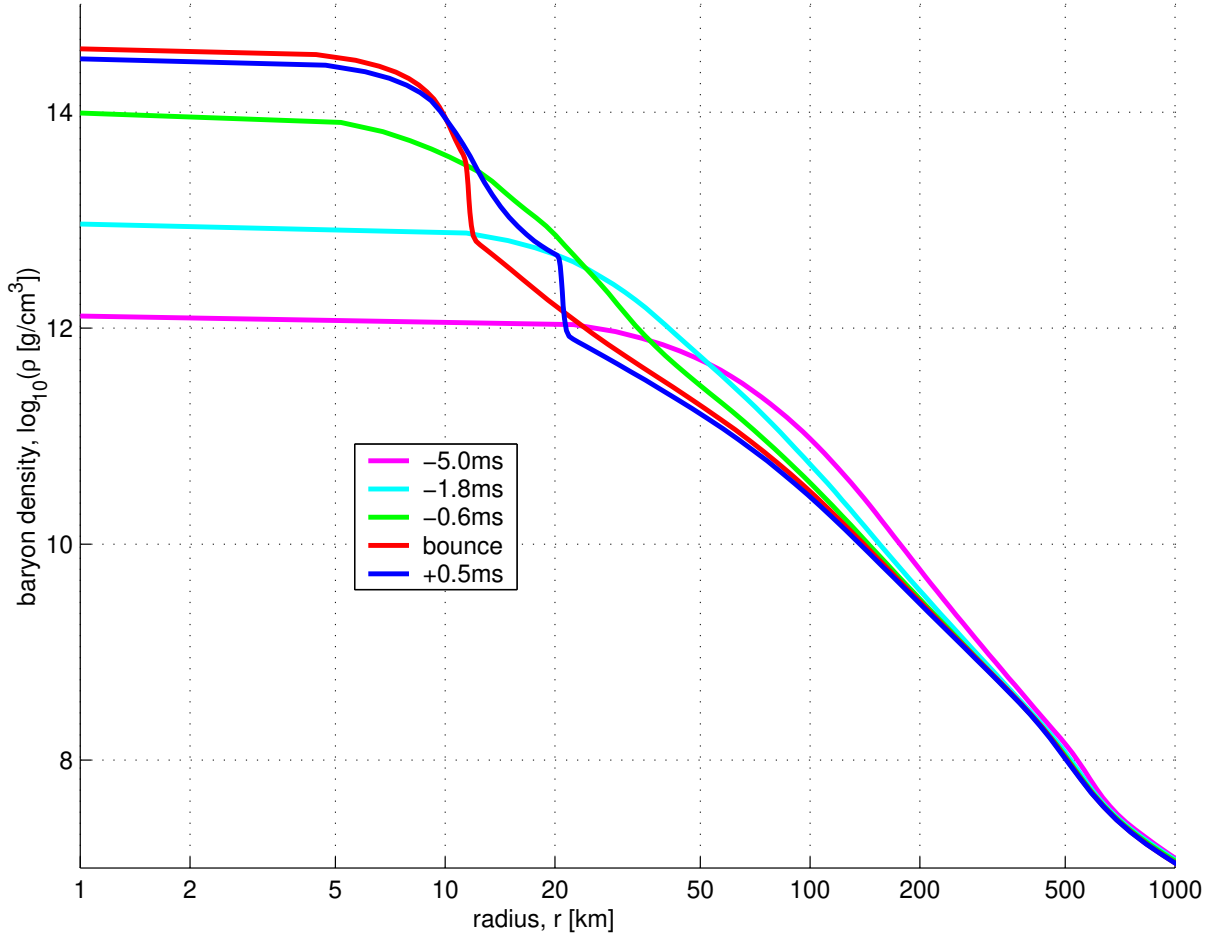


Figure 1: A sequence of density profiles of a $13 M_{\odot}$ star before and after core bounce. For such a relatively low mass supernova with a small Fe-core the bounce occurs at a maximum density of less than twice nuclear matter density. At bounce one recognizes the size of the homologous core (with roughly constant density). After bounce the emergence of an outward moving density (shock) wave can be witnessed.

explosion via neutrino heating is delayed after core collapse for a timescale of seconds or less. Aspects of the explosion mechanism are still uncertain and depend on Fe-cores from stellar evolution, electron capture rates of pf-shell nuclei, the supranuclear equation of state, as well as the details of neutrino transport [58] and Newtonian vs. general relativistic calculations [59, 49, 50]. The observational fact that many core collapse supernovae show polarized light emission also hints towards a nonspherical explosion mechanism [38].

3.2 Composition of Ejecta

As long as uncertainties are still existing in self-consistent models, but typical kinetic energies of 10^{51} erg are observed in supernova remnants, light curve as well as explosive nucleosynthesis calculations have been performed by introducing a shock of appropriate energy in the pre-collapse stellar model [113, 103, 32, 62, 106, 81]. Such induced calculations, making use of strong and weak interaction nuclear rates [37, 78, 79, 46], still lack self-consistency and cannot predict the ejected ^{56}Ni -masses from the innermost explosive Si-burning layers (powering supernova light curves by the decay chain ^{56}Ni - ^{56}Co - ^{56}Fe), due to the missing knowledge of the mass cut between the neutron star and the supernova ejecta. This relates also to the neutron-richness (or $Y_e = \langle Z/A \rangle$) of the ejected composition and the weak interactions during stellar evolution and the explosion.

Fig. 2 shows the composition after explosive processing [29, 103] due to the shock wave causing a supernova explosion. The outer ejected layers ($M(r) > 2M_\odot$) are unprocessed by the explosion and contain results of prior H-, He-, C-, and Ne-burning in stellar evolution. The interior parts of SNe II contain products of explosive Si, O, and Ne burning. In the inner ejecta, which experience explosive Si-burning, Y_e changes from 0.4989 to 0.494. The Y_e originates from beta-decays and electron captures in the pre-explosive hydrostatic fuel and possible alterations via neutrino reactions during the explosion in these layers. Huge changes occur in the Fe-group composition for mass zones below $M(r) = 1.63M_\odot$. There the abundances of ^{58}Ni and ^{56}Ni become comparable. All neutron-rich isotopes increase (^{57}Ni , ^{58}Ni , ^{59}Cu , ^{61}Zn , and ^{62}Zn), the even-mass isotopes (^{58}Ni and ^{62}Zn) show the strongest effect. One can also recognize the increase of ^{40}Ca , ^{44}Ti , ^{48}Cr , and ^{52}Fe for the inner high entropy zones, but a reduction of these $N=Z$ nuclei in the more neutron-rich layers. More details can be found in extended discussions [103, 104, 62].

Recent calculations [81, 24, 82] included all nuclides important for explosive stellar burning (with the exception of a possible r-process in the neutrino wind above the proto-neutron star, see Section 6.2) in an extended reaction network up to Bi. Thus, it became possible to follow the γ -process [111] (also known as the p-process [83]) self-consistently. Because of the high temperatures in the explosion previously produced heavy, stable isotopes can be photodisintegrated (mainly via (γ, n) and (γ, α) reactions) which leads to the formation of proton-rich stable isotopes, called the p-isotopes for historical reasons (indicated as P in Fig. 6). Currently, the γ -process is considered to be the source of the p-elements, however, the latest results may also still allow for a (currently hypothetical) additional contribution from type I X-ray bursts for the low mass p-nuclei (see Section 5.3).

A correct prediction of the amount of Fe-group nuclei ejected (which includes also one of the so-called alpha elements, i.e. Ti) and their relative composition depends directly on the explosion mechanism and the size of the collapsing Fe-core. Three types of uncertainties are inherent in the Fe-group ejecta, related to (i) the total amount of Fe(group) nuclei ejected and the mass cut between neutron star and ejecta, mostly measured by ^{56}Ni decaying to ^{56}Fe , (ii) the total explosion energy which influences the entropy of the ejecta and with it the amount of radioactive ^{44}Ti as well as ^{48}Cr , the latter decaying later to ^{48}Ti and being responsible for elemental Ti, and (iii) finally the neutron richness or $Y_e = \langle Z/A \rangle$ of the ejecta, dependent on stellar structure, electron captures and neutrino interactions. Y_e influences strongly the ratios of isotopes 57/56 in Ni(Co,Fe) and the overall elemental Ni/Fe ratio. The latter being dominated by ^{58}Ni and ^{56}Fe .

The pending understanding of the explosion mechanism also affects possible r-process yields for SNe II. Some calculations seemed to be able to reproduce the solar r-process abundances well in the high entropy neutrino wind, emitted from the hot protonneutron star after the SN II explosion [100, 115, 76]. However, present-day supernova models have difficulties to reproduce the entropies required for such abundance calculations and in addition face problems with abundance features in the mass range 80-120 [18]. The inclusion of non-standard neutrino properties may perhaps achieve low enough Y_e 's for intermediate entropies to correct for such unwanted features [56]. However, recent observations shed some doubts on the supernova origin. On average SNe II produce Fe to intermediate mass elements in ratios within a factor of 3 of solar. If they would also be responsible for the r-process, the same limits should apply. But the observed bulk r-process/Fe ratios vary

widely in low metallicity stars by more than a factor of 100 [95, 105].

4 Type Ia Supernovae

4.1 Thermonuclear Explosions

There are strong observational and theoretical indications that SNe Ia are thermonuclear explosions of accreting white dwarfs in binary stellar systems [31, 69, 68, 51]. High rates of H-accretion cause high temperatures at the base of the accreted matter and lead to quasi-stable H-burning and subsequent He-burning in shells surrounding the white dwarf, possibly related to supersoft X-ray sources. This increases the mass of the white dwarf consisting of C and O towards the maximum stable Chandrasekhar mass and leads to contraction.

Contraction causes carbon ignition in the central region and a thermonuclear runaway with a complete explosive disruption of the white dwarf [67, 112]. High accretion rates cause a higher central temperature and pressure, favoring lower ignition densities. A flame front then propagates at a subsonic speed as a deflagration wave due to heat transport across the front [65, 28]. Here the most uncertain quantity is the flame speed which depends on the development of instabilities of various scales at the flame front. Multi-dimensional hydro simulations of the flame propagation have suggested that a carbon deflagration wave might propagate at a speed v_{def} as slow as a few percent of the sound speed v_s in the central region of the white dwarf. The nucleosynthesis consequences of such slow flame speeds witness the actual burning front velocities and can thus serve as a constraint. Electron capture affects the central electron fraction Y_e , which determines the composition of the ejecta from such explosions. The amount of electron capture depends on (i) the electron capture rates of pf-shell nuclei, (ii) v_{def} , influencing the time duration of matter at high temperatures (and with it the availability of free protons for electron captures), and (iii) the central density of the white dwarf ρ_{ign} (increasing the electron chemical potential i.e. their Fermi energy) [34, 4, 46].

After an initial deflagration in the central layers, the deflagration can turn into a detonation (supersonic burning front) at lower densities [64]. The transition from a deflagration to a detonation (delayed detonation model) leads to a change in the ratios of Si-burning subcategories with varying entropies.

This also leaves an imprint on the Fe-group composition.

4.2 Nucleosynthesis Details

Nucleosynthesis constraints can help to find the "average" SN Ia conditions responsible for their contribution to galactic evolution, i.e. especially the Fe-group composition. SNe Ia contribute essentially no elements lighter than Al, about 1/3 of the elements from Si to Ca, and the dominant amount of Fe group nuclei (Ti to Ni). In addition, the average Fe-group yields of SNe II and SNe Ia differ.

Fig. 3 shows the influence of central ignition densities ρ_{ign} 1.37 (C) and 2.12×10^9 g cm⁻³ (W) at the onset of the thermonuclear runaway and slow (S) deflagration speeds of $v_{def}/v_s = 0.015$ (WS15, CS15), 0.03 (WS30, CS30) or 0.05 (CS50) on the resulting Y_e due to the different amount of electron capture [34]. Y_e values of 0.47-0.485 lead to dominant abundances of ⁵⁴Fe and ⁵⁸Ni, values between 0.46 and 0.47 produce dominantly ⁵⁶Fe, values in the range of 0.45 and below are responsible for ⁵⁸Fe, ⁵⁴Cr, ⁵⁰Ti, ⁶⁴Ni, and values below 0.43-0.42 are responsible for ⁴⁸Ca. The intermediate Y_e -values 0.47-0.485 exist in all cases, but the masses encountered which experience these conditions depend on the Y_e -gradient and thus v_{def} . Whether the lower values with $Y_e < 0.45$ are attained, depends on the central ignition density ρ_{ign} . Therefore, ⁵⁴Fe and ⁵⁸Ni are indicators of v_{def} while ⁵⁸Fe, ⁵⁴Cr, ⁵⁰Ti, ⁶⁴Ni, and ⁴⁸Ca are a measure of ρ_{ign} . These are the (hydrodynamic) model parameters. An additional uncertainty is the central C/O ratio of the exploding white dwarf [30]. Nuclear uncertainties based on electron capture rates are addressed in the following subsection.

4.3 The Effect of Electron Capture Rates

As the electron gas in white dwarfs is degenerate, characterized by high Fermi energies for the high density regions in the center, electron capture on intermediate mass and Fe-group nuclei plays an important role in explosive burning. Electron capture affects the central electron fraction Y_e , which determines the composition of the ejecta from such explosions. Recently new Shell Model Monte Carlo (SMMC) and large-scale shell model diagonalization calculations have been performed for pf-shell nuclei [13, 46]. These lead in general to a reduction of electron capture rates in comparison with previous, more phenomenological, approaches. Making use of these new shell

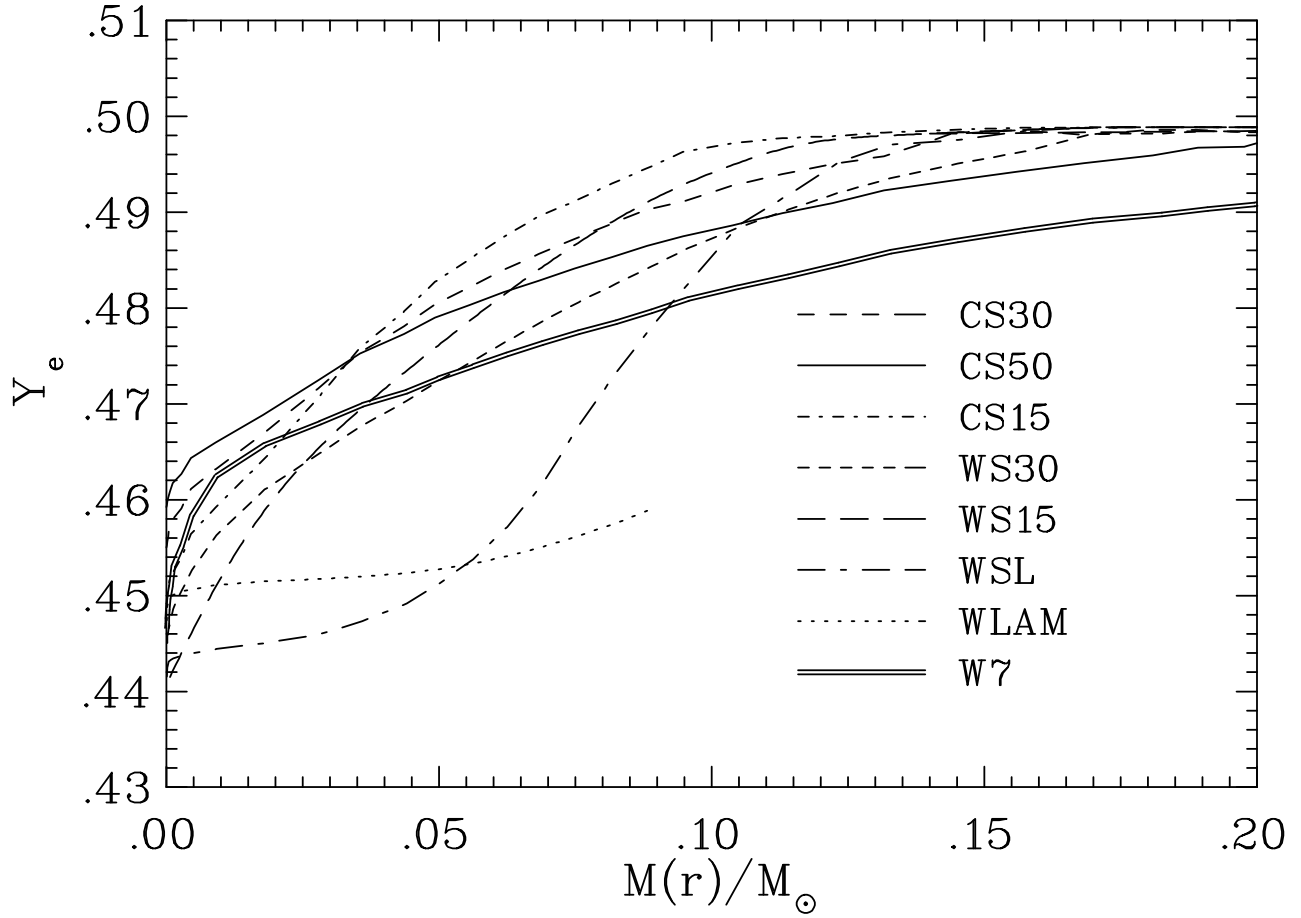


Figure 3: Y_e after freeze-out of nuclear reactions measures the electron captures on free protons and nuclei. Small burning front velocities lead to steep Y_e -gradients which flatten with increasing velocities (see the series of models CS15, CS30, and CS50 or WS15, WS30, and W7). Lower central ignition densities shift the curves up (C vs. W), but the gradient is the same for the same propagation speed. Only when the Y_e from electron captures is smaller than for stable Fe-group nuclei, subsequent β^- -decays will reverse this effect (WSL and WLAM).

model based rates, we present the results from Brachwitz et al. [4] for the composition of Fe-group nuclei produced in the central regions of SNe Ia and possible changes in the constraints on model parameters like ignition densities ρ_{ign} and burning front speeds v_{def} , superceding the results of Fig. 3 [34].

For a better understanding of the results we employed four rate sets: (i) The original FFN rates by Fuller et al. [20] as a benchmark for further comparisons; (ii) inclusion of the electron captures rates calculated within the SMMC method [13], replacing the corresponding FFN rates. SMMC rates were used for the parent nuclei ^{45}Sc , $^{48,50}\text{Ti}$, ^{51}V , $^{50,52}\text{Cr}$, ^{55}Mn , $^{54-56,58}\text{Fe}$, and $^{55,57,59}\text{Co}$, $^{56,58,60}\text{Ni}$, otherwise rates were taken from FFN; (iii) rates from large-scale shell model diagonalization calculations [46], labeled with SMFA. (iv) As a further option we treated even-even (ee), odd-A (oa), and odd-odd (oo) nuclei in different ways, in order to test the sensitivity of the models and the importance of the rates of particular nuclei. Such calculations are denoted by SMFA with the corresponding extension ee, oa, oo or by combinations, e.g. ee+oa. With these modifications of the electron capture rates, the nucleosynthesis for the SN Ia models WS15 and CS15 [34] was recalculated [4]. (It should be mentioned here that the SMMC rate set suffers from missing odd-odd nuclei.)

The resulting Y_e -curves (Fig. 4b) displays a small Y_e shift between SMMC and SMFAee+oa, and a larger Y_e -shift between SMFAee+oa and SMFA. Therefore, the inclusion of odd-odd nuclei has the largest influence on the Y_e difference between SMFA and SMMC. The rate change for odd-A nuclei is mostly responsible for the Y_e -shift between FFN and SMMC, and the inclusion of odd-odd nuclei causes the largest part of the Y_e -shift between SMMC and SMFA. Thus, the changes in the electron capture rates for odd-A and odd-odd nuclei are responsible for the Y_e difference between SMFA and FFN, while the contribution of even-even nuclei is negligible, an assertion which was directly tested by case SMFAee (Fig. 4b).

Notice, however, that the changes for a given model (here WS15 and CS15) lead to almost parallel Y_e -curves in the intermediate Y_e -range responsible for the major abundances of ^{54}Fe and ^{58}Ni . This can also be seen in the close to constant ΔY_e -curves in Fig. 4d. Thus, a change in electron capture rates does (to first order) not affect the Y_e -gradient of a model, which is therefore only determined by v_{def} [34]. Therefore, we can conclude that the consequences for the permitted range of burning front speeds remain the same. The conclusions to be drawn from these results are that: (i) v_{def} in the

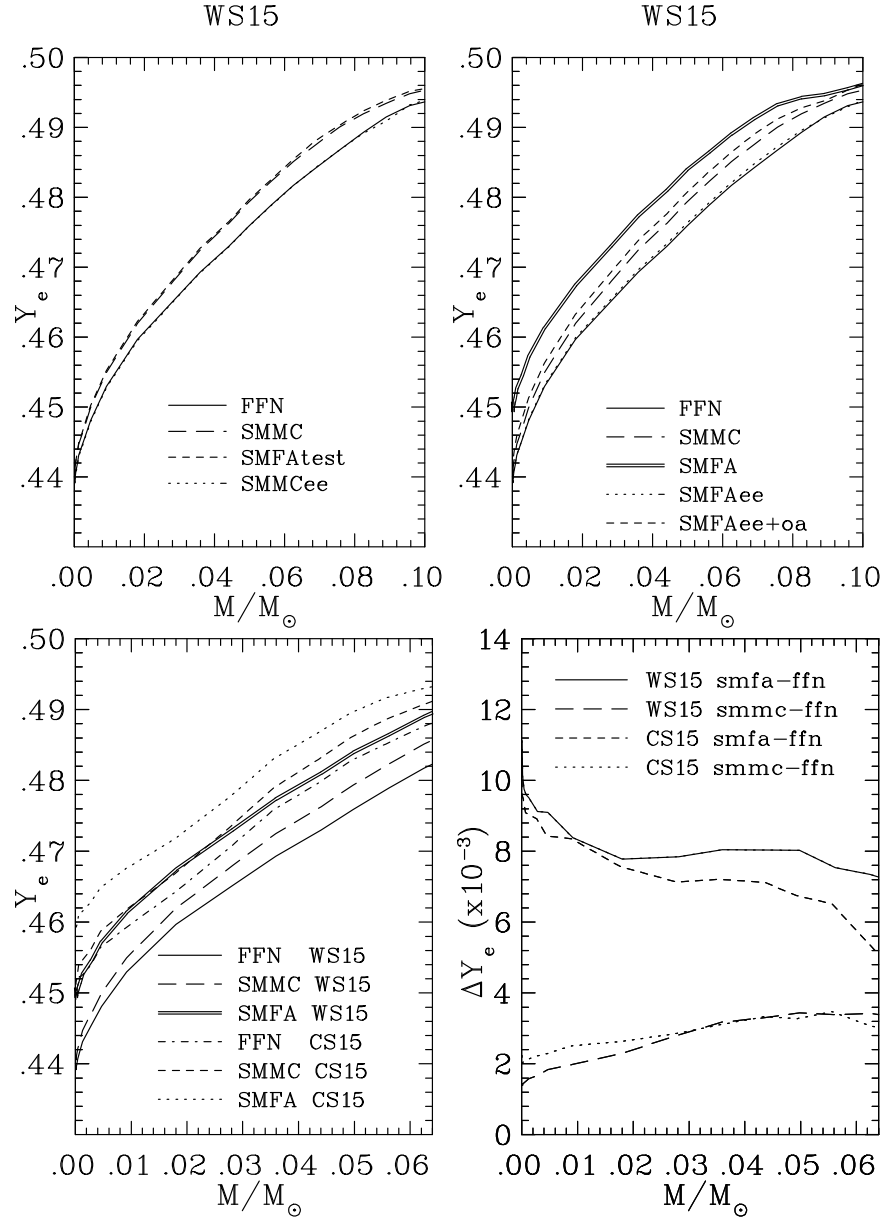


Figure 4: Y_e , the total proton to nucleon ratio and thus a measure of electron captures on free protons and nuclei, after freeze-out of nuclear reactions, as a function of radial mass for different models and electron capture rates. Also the Y_e -difference ΔY_e between various cases is shown at the bottom right (d). A detailed discussion of the changes with different electron capture rate sets is given in the text.

range 1.5–3% of the sound speed is preferred (cases 15 and 30 over 50) [34], and (ii) the change in pf-shell electron capture rates [46] made it possible to have ignition densities as high as $\rho_{ign}=2 \times 10^9 \text{ g cm}^{-3}$ without distroying the agreement with solar abundances of very neutron-rich species [34, 4]. It seems, however, hard to produce amounts of ^{48}Ca sufficient to explain solar abundances in the exploding white dwarfs with these changes and more realistic C/O ratios [114, 5].

5 The rp-Process and X-ray Bursts

5.1 Explosive hydrogen burning

The major astrophysical events which involve explosive H-burning are novae and type I X-ray bursts. Both are related to binary stellar systems with hydrogen accretion from a binary companion onto a compact object, and the explosive ignition of the accreted H-layer. High densities cause the pressure to be dominated by the degenerate electron gas, preventing a stable and controlled burning. In the case of novae the compact object is a white dwarf, in the case of X-ray bursts it is a neutron star. Explosive H-burning in novae has been discussed in many recent articles [36, 96, 97, 9]. Its processing is limited due to maximum temperatures of $\sim 3 \times 10^8 \text{ K}$. Only in X-ray bursts temperatures larger than $4 \times 10^8 \text{ K}$ are possible.

5.2 Type I X-ray bursts

In type I X-ray bursts [98, 48, 99, 93, 110] hydrogen (and helium) burn explosively in a thermonuclear runaway. In essentially all nuclei below Ca, the proton capture reaction on the nucleus $(Z_{even}-1, N=Z_{even})$ produces the compound nucleus above the alpha-particle threshold and permits a (p, α) reaction. This is typically not the case for $(Z_{even}-1, N=Z_{even}-1)$ due to the smaller proton separation energy, which leads to hot CNO-type cycles above Ne [102]. There is one exception, $Z_{even}=10$, where the reaction $^{18}\text{F}(p, \alpha)$ is possible, avoiding ^{19}F and a possible leak via $^{19}\text{F}(p, \gamma)$ into the NeNaMg-cycle. This has the effect that only alpha induced reactions like $^{15}\text{O}(\alpha, \gamma)$ can aid a break-out from the hot CNO-cycle to heavier nuclei beyond Ne [109]. Break-out reactions from the hot CNO-type cycles above Ne proceed typically via proton captures on the nucleus $(Z_{even}, N=Z_{even}-1)$ [102, 85]. They occur

at temperatures of about $3 \times 10^8 \text{K}$, while the alpha-induced break-out from the hot CNO-cycle itself is delayed to about $4 \times 10^8 \text{K}$.

In the next stage of the ignition process also He is burned via the 3α -reaction and the αp -process (a sequence of (α, p) and (p, γ) reactions), which provides seed nuclei for hydrogen burning via the rp-process (proton captures and beta-decays). Processing of the rp-process beyond ^{56}Ni is shown in Fig. 5 [93]. Certain nuclei play the role of long waiting points in the reaction flux, where long beta-decay half-lives dominate the flow, either competing with slow (α, p) reactions or negligible (p, γ) reactions, because they are inhibited by inverse photodisintegrations for the given temperatures. Such nuclei were identified as ^{25}Si ($\tau_{1/2}=0.22\text{s}$), ^{29}S (0.187s), ^{34}Ar (0.844s), ^{38}Ca (0.439s) [110]. The bottle neck at ^{56}Ni can only be bridged for minimum temperatures around 10^9K (in order to overcome the proton capture Coulomb barrier), maximum temperatures below $2 \times 10^9 \text{K}$ (in order to avoid photodisintegrations), and high densities exceeding 10^6g cm^{-3} [93, 84]. If this bottle neck can be overcome, other waiting points like ^{64}Ge (64s), ^{68}Se (96s), ^{74}Kr (17s) seem to be hard to pass. However, partially temperature dependent half-lives (due to excited state population), or mostly 2p-capture reactions (introduced in [21] and applied in [93]) can help.

5.3 The final composition

The initial break-out reactions from hot CNO-type cycles and the hold-ups at waiting points introduce a time structure in energy generation. One of the essential questions is whether they can/will show up in the X-ray light-curves of bursts. The other question is whether individual proton-capture reactions matter, because at peak temperatures (p, γ) - (γ, p) equilibria are attained, leading to an equilibrium distribution along isotonic lines, where only beta-decays might matter. The latter was claimed [33] based on an X-ray burst temperature profile provided by F. Rembges [86]. This paper showed (as should be expected from the late equilibrium conditions) that with a given temporal temperature profile the resulting composition does not depend on individual reactions. Thus, the important question is whether the feedback from hydrodynamics, due to the changed energy input in the early ignition stages when the break-out reactions occur, leads to different temperature profiles and thus different final abundances.

The results of a self-consistent calculation can be seen in Fig. 6 from [86, 87, 80] which shows the radius of the burning shell, the velocity, the lu-

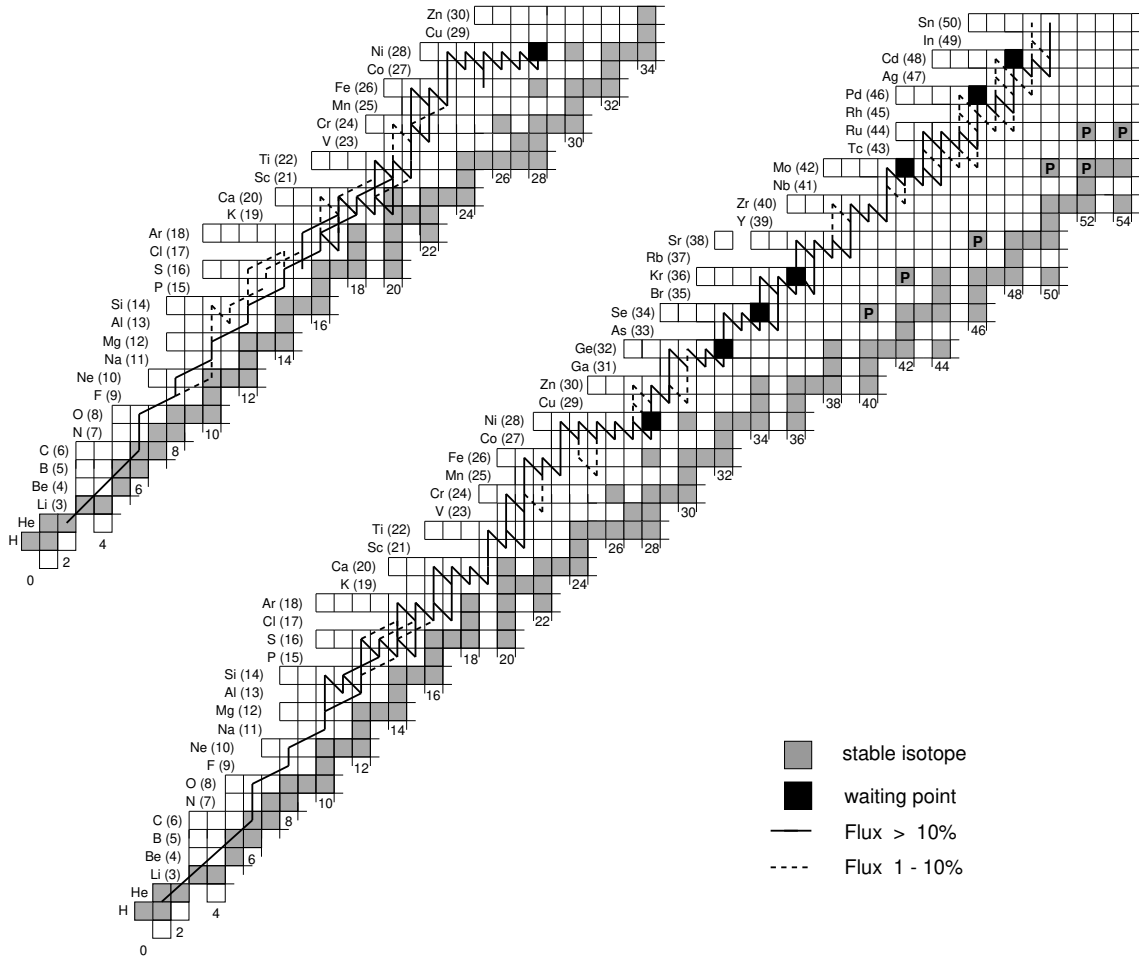


Figure 5: rp and α p-process flow up to and beyond Ni. The reaction flows shown in the nuclear chart are integrated reaction fluxes from a time dependent network calculation [93], (a) during the initial burst and thermal runaway phase of about 10s, (b) after the onset of the cooling phase when the proton capture on ^{56}Ni is not blocked anymore by photodisintegrations (extending for about 200s). Waiting points above ^{56}Ni are represented by filled squares, stable nuclei by hatched squares, light p-process nuclei below $A=100$ are indicated by P .

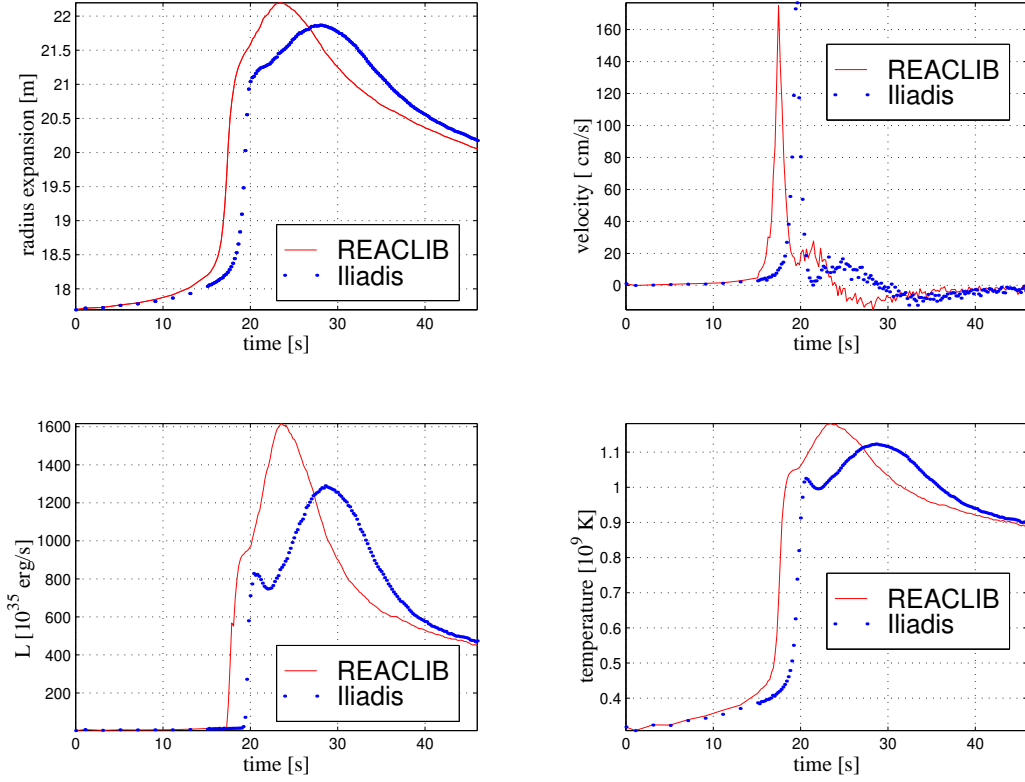


Figure 6: Comparison of burst profiles with different proton capture rates for the break-out reactions on ^{27}Si , ^{31}S , ^{35}Ar , and ^{38}Ca in a self-consistent X-ray burst model [86, 87]. Due to different rates the burning of matter beyond Ne is burned on different timescales, causing a different pre-expansion before the maximum temperature are attained in alpha-induced reactions.

minosity, and the temperature. The difference between calculations with the old REACLIB rates [101] and the ones with updated cross sections for the break-out points ^{27}Si , ^{31}S , ^{35}Ar , and ^{38}Ca emerges at the expected temperatures of $(3 - 4) \times 10^8\text{K}$, when these break-out reactions occur. At that point the nuclei beyond Ne will burn towards Ni/Fe. This energy input causes the temperature increase which will then permit the hot CNO break-out via alpha-induced reactions and later on also the triple-alpha link to ^{12}C . This leads to the burning of ^4He and the temperature peak for the rp-process with a chemical equilibrium for proton-capture reactions. However, as the initial break-out phase differs, different pre-expansions occur, causing different densities and also different peak temperatures.

A similar effect was found recently in further self-consistent burst calculations [16, 87], when REACLIB rates in the mass range $A=44-63$ were replaced by cross sections based on predictions of resonance properties from shell model calculations [17]. These effects are even more drastic, again due to the early burning phase when matter beyond Ne burns up to Fe, before the alpha-captures begin. This shows that a more precise determination of specific reaction rates is important, when self-consistent network plus hydrodynamics calculations are performed. The peak temperatures and densities attained in X-ray burst calculations depend on this cross sections input.

If only a small percentage of the synthesized matter escapes the strong gravitational field of the neutron star, some proton-rich stable nuclei (p-process nuclei) below $A=100$ (indicated as P in Fig.5) could be explained in the solar system abundances.

6 The r-Process

6.1 Abundances and Nuclear Properties far from Stability

Site-independent classical analyses, based on neutron number density n_n , temperature T , and duration time τ , led to the conclusion that the r-process experienced a fast drop from an $(n, \gamma) - (\gamma, n)$ chemical equilibrium in each isotopic chain. The combination of n_n and T determines an r-process path in the nuclear chart along nuclei with a neutron separation energy $S_n(n_n, T)$. Thus, the r-process and its abundance features probe nuclear structure far from stability via mass properties and the beta-decay half-lives along con-

four lines of constant S_n [41]. This gives some indication for the need of quenching of nuclear shell effects far from stability [72, 42, 43]. A continuous superposition of components with neutron separation energies in the range 1–4 MeV on timescales of 1–2.5 s, provides a good overall fit [10]. For the heavier elements beyond $A=130$ this is reduced to about $S_n=1-3$ MeV. These are predominantly nuclei not accessible in laboratory experiments to date. Exceptions exist in the $A = 80$ and 130 peaks and continuous efforts are underway to extend experimental information in these regions of the closed shells $N=50$ and 82 with radioactive ion beam facilities [42]. A recent detailed analysis of the $A=206-209$ abundance contributions to Pb and Bi isotopes from alpha-decay chains of heavier nuclei permitted for the first time also to predict abundances of nuclei as heavy as Th with reasonable accuracy [10]. These results are shown in Fig. 7.

The endpoint of the r-process path is determined by β -delayed fission when the path reaches fissionable nuclei. Fission fragments may alter not only the heavy element abundances but may also give rise to an exponential enhancement of the general r-process abundances, in sites where an extended duration of the high-flux neutron supply leads to fission cycling, such as in some inhomogeneous big bang models [77] or neutron star mergers (see the next section). The knowledge of fission barriers and an improved theoretical treatment of β -delayed fission (involving fission of highly excited nuclei) is crucial for the future investigation of these effects.

6.2 Possible Stellar r-Process Sites

A different question is related to the actual astrophysical realization of such conditions. The observations of stellar spectra of low metallicity stars, stemming from the very early phases of galactic evolution, are all consistent with a solar r-abundance pattern for elements heavier than Ba, and the relative abundances among heavy elements apparently do not show any time evolution [10, 95]. This suggests that all contributing events produce the same relative r-process abundances for the heavy masses, although a single astrophysical site will still have varying conditions in different ejected mass zones, leading to a superposition of individual components.

However, from meteoritic abundances and observations in low metallicity stars we also know by now that at least two r-process sources have to contribute to the solar r-process abundances [107, 95]. The observed non-solar r-process pattern for e.g. Ag, I, and Pd in some objects indicate the need

for a second r-process component in the nuclear mass range $A \approx 80-120$, in addition to the main process which provides a solar r-process pattern beyond Ba [95]. It is not exactly clear which of the two processes is related to SNe II and which one is related to possible other sources.

An r-process requires 10 to 150 neutrons per seed nucleus (in the Fe-peak or somewhat beyond) which have to be available to form all heavier r-process nuclei by neutron capture. For a composition of Fe-group nuclei and free neutrons that translates into a $Y_e = \langle Z/A \rangle = 0.12-0.3$. Such a high neutron excess is only possible for high densities in neutron stars under beta equilibrium ($e^- + p \leftrightarrow n + \nu$, $\mu_e + \mu_p = \mu_n$), based on the high electron Fermi energies which are comparable to the neutron-proton mass difference. Neutron star mergers which eject such matter are a possible (low entropy) site [18] and have been debated in the past. Recent calculations show that on average about $10^{-2} M_\odot$ of neutron-rich matter are ejected [90, 91]. This amount depends on the central high density equation of state [74] encountered in these events. Present calculations show densities up to four times nuclear matter density and temperatures of up to 50 MeV [90, 91]. First nucleosynthesis calculations with assumptions on Y_e predict a solar-type r-process pattern for nuclei beyond $A=130$ [19], shown in Fig. 8. The smaller masses are depleted due to a long duration r-process with a large neutron supply in such neutron-rich matter, which also leads to fission cycling [70]. This seems (accidentally?) in accordance with the main observed r-process component. Given the frequency (10^{-5}y^{-1} per galaxy) and amount of ejected matter, this component alone could be responsible for the heavy solar r-process pattern and also explain the large scatter of r/Fe elements found in low metallicity stars [105]. Neutron star - black hole mergers have not yet been analyzed with the same accuracy, but bear similar options.

Another option is an extremely alpha-rich (i.e. high entropy) freeze-out in complete Si-burning with moderate $Y_e > 0.40$, which however faces some of the problems already mentioned in the section on SNe II [18, 56]. A discussion of the advantages and disadvantages of both possible r-process sources (SNe II vs. neutron star mergers) is given in refs. [75, 92].

7 Conclusions

This overview concentrated on nuclear physics issues important in stellar evolution, supernovae (type II and Ia), X-ray bursts and the rp-process, and

analyzed the options and sites of r-process nucleosynthesis. These are the major contributions to galactic evolution. Nucleosynthesis calculations have a right on their own to predict abundance patterns for many stellar events, but they can also serve as a tool to test the correctness of model descriptions, either in comparison to direct observations or indirect information from galactic evolution. We tried to show (especially for SNe Ia and II), how specific isotopic abundances can test ignition densities, burning front velocities or explosion energies, entropies, and temperatures. These are the astrophysical model constraints. But it was also clearly demonstrated how advances in nuclear physics (nuclear reaction cross sections, weak interaction rates in the pf-shell, neutrino-nucleus interactions, decay properties far from stability, nuclear structure far from stability, fission properties and yields, the nuclear equation of state at high densities and temperatures) are essential for the outcome and correct modeling of these events.

This review would not have been possible without discussing and presenting results from joint collaborations with J.J. Cowan, D. Dean, R.D. Hoffman, K. Iwamoto, F. Käppeler, M. Strayer, J.W. Truran, and S.E. Woosley.

References

- [1] Adelberger, E.G. et al. 1998, *Rev. Mod. Phys.* 70, 1265
- [2] Angulo, C. et al. 1999, *Nucl. Phys. A.* 656, 3
- [3] Bonetti, R. et al. 1999, *Phys. Rev. Lett.* 82, 5205
- [4] Brachwitz, F. et al. 2000, *Ap. J.*, 536, 934
- [5] Brachwitz, F. et al. 2001, Ph. D. thesis, Univ. of Basel, unpublished
- [6] Bruenn, S.W., Haxton, W.C. 1991, *Ap. J.* 376, 678
- [7] Burrows, A., Sawyer R.F. 1999, *Phys. Rev. C*59, 510
- [8] Chieffi, A., Limongi, M., Straniero, O. 1998, *Ap. J.* 502, 737
- [9] Coc, A., Hernanz, M., José, J., Thibaud, J.P. 2000, *A & A* 357, 561
- [10] Cowan, J.J. et. 1999, *Ap. J.* 521, 194
- [11] Cowan, J. J., Thielemann, F.-K., Truran, J. W. 1991, *Phy. Rep.*, 208, 267
- [12] Dappen, W., Nayfonov, A. 2000, *Ap. J. Suppl.* 127, 287
- [13] Dean, D.J. et al. 1998, *Phys. Rev. C*58, 536
- [14] Dobaczewski, J. 1999, *Acta Phys. Pol. B* 30, 1647

- [15] Dorfi, E.A. 1999, JCAM 109, 153
- [16] Fisker, J.L. et al. 2000, At. Data Nucl. Data Tables, submitted
- [17] Fisker, J.L., Rembges, F., Barnard, V., Wiescher, M. 2001, Nucl. Phys. A, in press
- [18] Freiburghaus, C. et al. 1999, Ap. J. 516, 381
- [19] Freiburghaus, C., Rosswog, S., Thielemann, F.-K. 1999, Ap. J. 525, L121
- [20] Fuller, G.M., Fowler, W.A., Newman, M. 1985, Ap. J. 293, 1
- [21] Görres, J., Wiescher, M., Thielemann, F.-K. 1995, Phys. Rev. C51, 392
- [22] Goriely, S. 1998, Phys. Lett. B 436, 10
- [23] Hashimoto, M., Iwamoto, K., Nomoto, K., 1993, Ap. J. 414, L105
- [24] Heger, A., Hoffman, R.D., Rauscher, T., Woosley, S.E. 2000, in *Proc. X Workshop on Nuclear Astrophysics*, eds. W. Hillebrandt, E. Müller, MPA/P12 Garching, p. 105 (astro-ph/0006350)
- [25] Heger, A., Langer, N., Woosley, S.E. 2000, Ap. J., 528, 368
- [26] Heger, A., Langanke, K., Martinez-Pinedo, G., Woosley, S.E. 2000, submitted to Phys. Rev. Lett.
- [27] Hektor, A. et al. 2000, Phys. Rev. C 61, 055803
- [28] Hillebrandt, W., Niemeyer, J.C. 2000, Ann. Rev. of Astron. Astrophys., in press
- [29] Hix, W.R., Thielemann, F.-K. 1999, J. Comp. Appl. Math. 109, 321
- [30] Höflich, P. 2001, in 1st KIAS Astrophysics Workshop, Seoul/Corea, IAP-Publishing, ed. I. Yi, in press
- [31] Höflich, P., Khokhlov, A. 1996, Ap. J., 457, 500
- [32] Hoffman, R.D. et al. 1999, Ap. J. 521, 735
- [33] Iliadis, C., Endt, P.M., Prantzos, N., Thompson, W.J. 1999, Ap. J. 524, 434
- [34] Iwamoto, K. et al. 1999, Ap. J. Suppl. 125, 439
- [35] Janka, H.-T., Müller, E. 1996, A&A, 306, 167
- [36] José, J., Coc, A., Hernanz, M. 1999, Ap. J. 520, 342
- [37] Käppeler, F., Thielemann, F.-K., Wiescher, M. 1998, Ann. Rev. Nucl. Part. Sci. 48, 175
- [38] Khokhlov, A.M. et al. 1999, Ap. J. 524, L107
- [39] Kolbe, E. 2000, Acta. Phys. Pol. B 31, 1237

- [40] Kolbe, E., Kosmas, T.S. 2000, in *Recent Highlights on Neutrino-Nucleus Interactions*, Springer Tracts in Modern Physics 163
- [41] Kratz, K.-L. et al. 1993, Ap. J. 402, 216
- [42] Kratz, K.-L., Pfeiffer, B., Thielemann, F.-K., Walters, W.B. 2000, Hyperfine Interactions 129, 185 (astro-ph/9907071)
- [43] Kratz, K.-L. et al. 2001, Nucl. Phys. A, in press
- [44] Lalazissis, G.A. et al. 1999, Phys. Rev. C 60, 4310
- [45] Langanke, K., Kolbe, E. 2000, At. Data Nucl. Data Tables, in press
- [46] Langanke, K., Martinez-Pinedo, G. 2000, Nucl. Phys. A673, 481
- [47] Lattimer, J.M., Swesty, F.D. 1991, Nucl. Phys. A535, 331
- [48] Lewin, W.H.G., van Paradijs, J., Taam, R.E. 1993, Space Sci. Rev. 62, 223
- [49] Liebendörfer, M. et al. 2000, astro-ph/0006418, subm. to Phys. Rev. D
- [50] Liebendörfer, M., Mezzacappa, A., Thielemann, F.-K. 2000, subm. to Phys. Rev. D
- [51] Livio, M. 2000 in *Type Ia Supernovae: Theory and Cosmology*, Cambridge Univ. Press, in press
- [52] Mamdouh, A. et al. 1999, Nucl. Phys. A 648, 282
- [53] Maeder, A., Zahn, J.P. 1998, A & A 334, 1000
- [54] Martinez-Pinedo, G., Langanke, K. 1999, Phys. Rev. Lett. 83, 4502
- [55] Martinez-Pinedo, G. et al. 2000, ApJS, 126, 493
- [56] McLaughlin, G.C. et al. 1999, Phys. Rev. C59, 2873
- [57] Messer, O.E.B. et al. 1998, ApJ 507, 353
- [58] Mezzacappa, A., Messer, O.E.B. 1999, J. Comp. Appl. Math. 109, 281
- [59] Mezzacappa, A. et al. 2000, astro-ph/0004059, PRL, in press
- [60] Möller, P., Nix, J.R., Myers, W.D., Swiatecki, W.J. 1995, At. Data Nucl. Data Tables 59, 185
- [61] Möller, P., Nix, J.R., Kratz, K.-L. 1997, At. Data Nucl. Data Tables 66, 131
- [62] Nakamura, T. et al. 1999, Ap. J. 517, 193
- [63] Nazarewicz, W. 2000, this volume
- [64] Niemeyer, J.C. 1999, Ap. J. 523, L57
- [65] Niemeyer, J.C., Bushe, W. K., Ruetsch, G.R. 1999, Ap. J. 524, 290

- [66] Nomoto, K., Hashimoto, M. 1988, Phys. Rep. 163,
- [67] Nomoto, K., Thielemann, F.-K., Yokoi, K. 1984, Ap. J. 286, 644
- [68] Nomoto, K. et al. 2000, in *Type Ia Supernovae: Theory and Cosmology*, Cambridge Univ. Press, eds. J. Niemeyer & J.W. Truran, in press (astro-ph/9907386)
- [69] Nugent, P. et al. 1997, Ap. J. 485, 812
- [70] Panov, I., Freiburghaus, C., Thielemann, F.-K. 2001, Nucl. Phys. A, in press
- [71] Pearson, J. M., Nayak, R. C., Goriely, S. 1996, Phys. Lett. B387, 455
- [72] Pfeiffer, B., Kratz, K.-L., Thielemann, F.-K. 1997, Z. Phys. A357, 235
- [73] Pons, J.A. et al. 1999, Ap. J. 513, 780
- [74] Prakash, M. et al. 1997, Phys. Rep. 280, 1
- [75] Qian, Y.-Z., Ap. J. 534, L67
- [76] Qian, Y.-Z., Woosley, S. E. 1996, Ap. J., 471, 331
- [77] Rauscher, T. et al. 1994, Ap. J., 429, 499
- [78] Rauscher, T., Thielemann, F.-K. 2000, At. Data Nucl. Data Tables, 75, 1
- [79] Rauscher, T., Thielemann, F.-K., Görres, J. Wiescher, M. 2000, Nucl. Phys. A675, 695
- [80] Rauscher, T., Rembges, F., Schatz, H., Wiescher, M., Thielemann, F.-K. 2000, in *The beta Decay, from Weak Interaction to Nuclear Structure*, eds. P. Dessagne, A. Michalon, C. Miché, IRes Strasbourg, p. 51
- [81] Rauscher, T., Heger, A., Hoffman, R.D., Woosley, S.E. 2001, Nucl. Phys. A, in press (astro-ph/0010021)
- [82] Rauscher, T., Heger, A., Hoffman, R.D., Woosley, S.E. 2001, Ap. J., in preparation
- [83] Rayet, M., Arnould, M., Prantzos, N. 1990, A&A 227, 517
- [84] Rehm, E. et al. 1998, Phys. Rev. Lett. 80, 676
- [85] Rembges, F., Freiburghaus, C., Rauscher, T., Thielemann, F.-K., Schatz, H., Wiescher, M. 1997, Ap. J. 484, 412
- [86] Rembges, F. 1999, Ph.D. thesis, Univ. Basel, unpublished
- [87] Rembges, F. et al. 2000, in preparation
- [88] Rogers, F.J., Iglesias, C.A. 1998, Space Sci. Rev. 85, 61

- [89] Rolfs, C. 2000, this volume
- [90] Rosswog, S.K. et al. 1999, A&A 341, 499
- [91] Rosswog, S.K. et al. 2000, A&A, 360, 171
- [92] Rosswog, S.K., Freiburghaus, C., Thielemann, F.-K. 2001, Nucl. Phys. A, in press
- [93] Schatz, H. et al. 1998, Phys. Rep. 294, 167
- [94] Shen, H. et al. 1998, Prog. Theor. Phys. 100, 1013
- [95] Sneden, C. et al. 2000, Ap. J. 533, 139
- [96] Starrfield, S. 1999, Phys. Rep. 311, 371
- [97] Starrfield, S., Sparks, W.M., Truran, J.W., Wiescher, M. 2000, Ap. J. Suppl. 127, 485
- [98] Taam, R.E. 1985, Ann. Rev. Nucl. Part. Sci. 35, 1
- [99] Taam, R.E., Woosley, S.E., Lamb, D.Q. 1996, Ap. J. 459, 271
- [100] Takahashi, K., Wittl, J., Janka, H.-T. 1994, A&A, 286, 857
- [101] Thielemann, F.-K., Arnould, M., Truran, J. W. 1987, in *Advances in Nuclear Astrophysics*, ed. E. Vangioni-Flam, Gif sur Yvette, Editions Frontière, p.525
- [102] Thielemann, F.-K., Kratz, K.-L., Pfeiffer, B., Rauscher, T., van Wormer, L., & Wiescher, M. C. 1994, Nucl. Phys. A570, 329c
- [103] Thielemann, F.-K., Nomoto, K., Hashimoto, M. 1996, Ap. J. 460, 408
- [104] Thielemann, F.-K. et al. 1998, in *Nuclear and Particle Astrophysics*, eds. J. Hirsch, D. Page, Cambridge Univ. Press, p. 27
- [105] Truran, J.W., Cowan, J.J., Sneden, C., Burris, D.L., Pilacowski, C.A., in *The First Stars*, Springer, eds. A. Weiss et al., in press
- [106] Umeda, H., Nomoto, K., Nakamura, T. 2000, in *The First Stars*, Springer, eds. A. Weiss et al., in press (astro-ph/9912248)
- [107] Wasserburg, G., Busso, M., Gallino, R. 1996, Ap. J. 466, L109
- [108] Weber, F. 1999, Pulsars as Astrophysical Laboratories of Nuclear and Particle Physics, IOP Publishing, Bristol
- [109] Wiescher, M., Görres, J., Schatz, H. 1999, J. Phys. G. 25, R133
- [110] Wiescher, M., Schatz, H. 2000, Prog. Theor. Phys. Supp. 140, 11
- [111] Woosley, S.E., Howard, W.M. 1978, Ap. J. Suppl. 36, 285

- [112] Woosley, S.E., Weaver, T.A. 1994, in *Les Houches, Session LIV, Supernovae*, eds. S.R. Bludman, R. Mochkovitch, J. Zinn-Justin, Elsevier Science Publ., p. 63
- [113] Woosley, S.E., Weaver, T.A. 1995, *Ap. J. Suppl.* 101, 181
- [114] Woosley, S.E. 1997, *Ap. J.* 476, 801
- [115] Woosley, S.E. et al. 1994, *Ap. J.* 433, 229
- [116] Yamada, S., Toki, H. 2000, *Phys. Rev. C* 6101, 5803

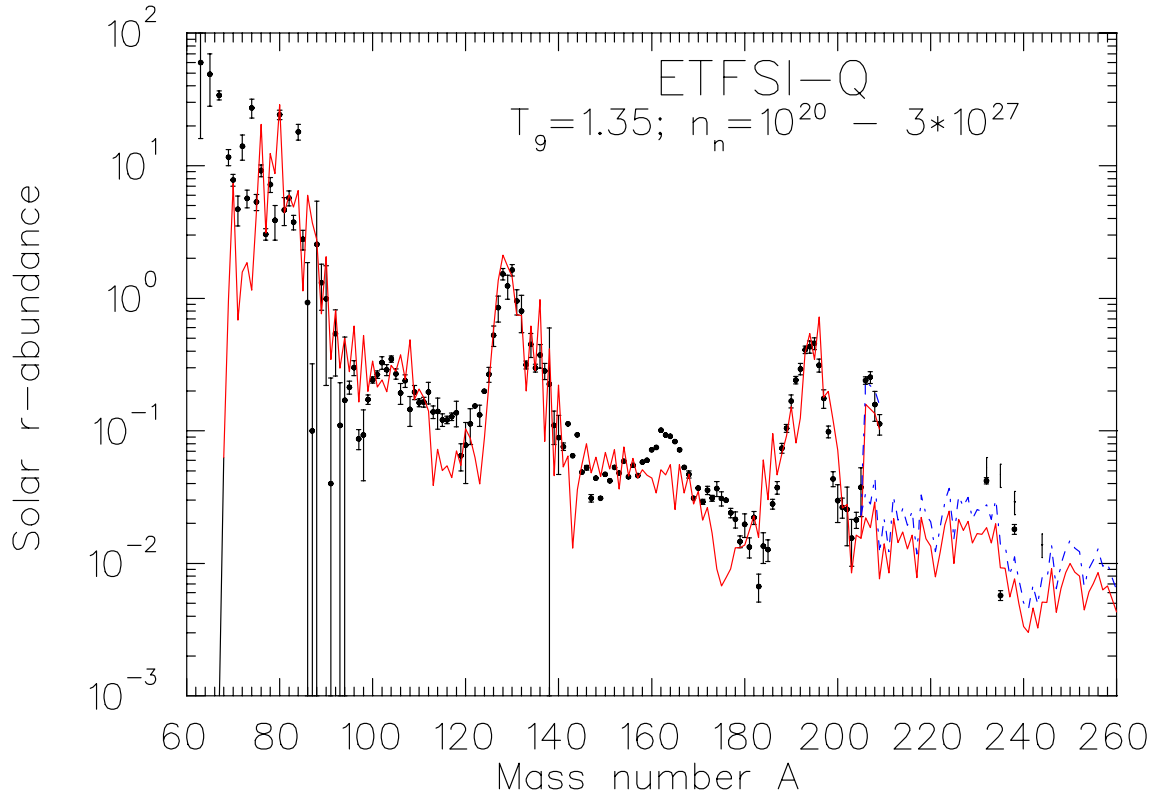


Figure 7: Fits to solar r-process abundances, obtained with two different smooth superposition of 17 equidistant $S_n(n_n, T)$ components from 1 to 4 MeV (solid and dashed lines). The ETFISI-Q mass model [71] was applied, which introduces a phenomenological quenching of shell effects. The quenching of the $N = 82$ shell gap avoids a large abundance trough below the $A=130$ peak. These results also show a good fit to the r-process Pb and Bi contributions after following the decay chains of unstable heavier nuclei (indicated by two sets of abundances for $A > 205$).

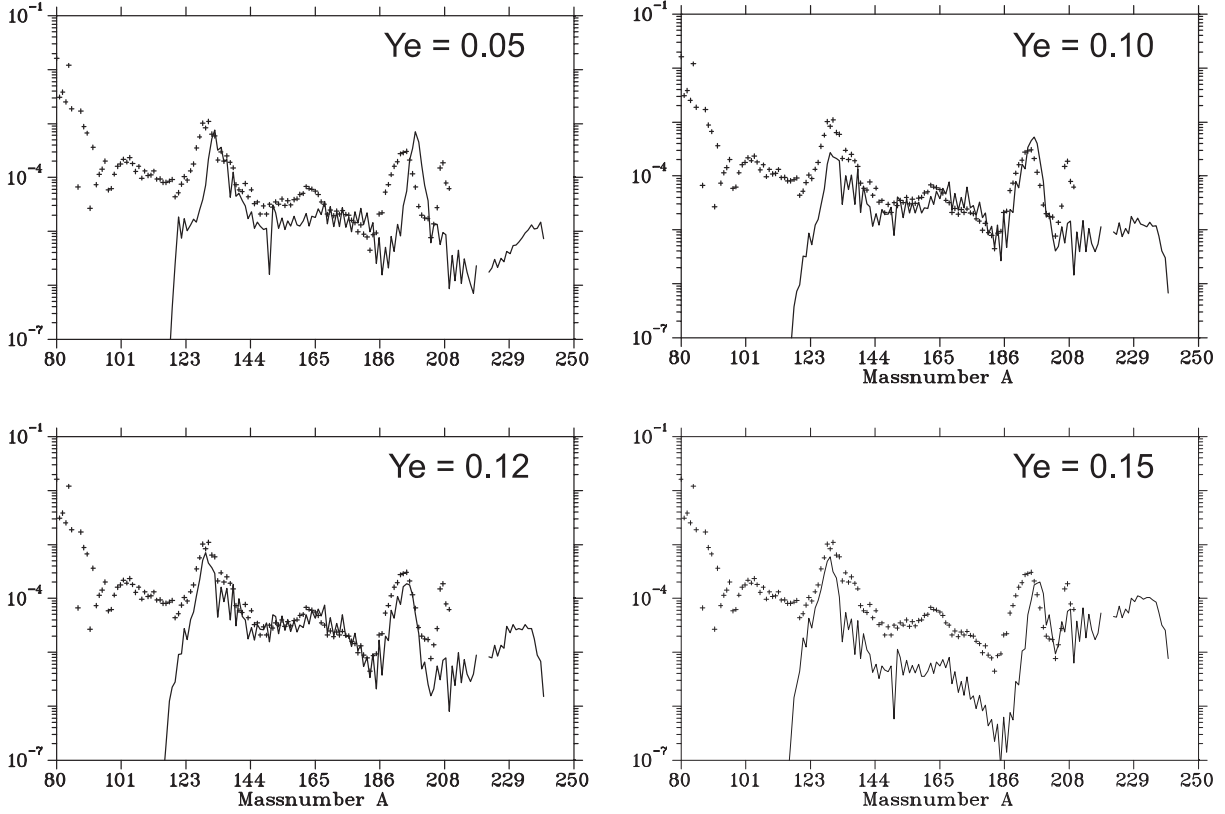


Figure 8: Calculated r-process distribution for different Y_e 's. In general one obtains useful contributions for $0.08 < Y_e < 0.15$. A further discussion is given in the text. Y_e determines the total neutron/seed ratio, which is an indication of the strength of the r-process. It affects also the combination of n_n and T , i.e. the r-process path, and therefore the position of peaks. Finally, fission cycling is responsible for the drop of abundances below $A=130$, but only an improved incorporation of fission barriers and yields will provide the correct abundance distribution in this mass range.